SUPPLEMENTARY METHODS

Antibodies

α-His_6 and α-GST antibodies were obtained from Novagen and GE Healthcare, respectively. α-HA (3F10) and α-Myc (9E10) were purchased from Roche. The secondary antibody was a commercial horseradish peroxidase (HRP)-conjugated goat anti-rabbit antibody (Sigma-Aldrich).

Plasmid construction

The DNA fragment encoding CSa (residues 149–253) was incorporated to create His_6 or His_6/GST fusion proteins in the pET28 or pETM30 expression vector, respectively (Novagen; Gunter Stier, EMBL, Germany). The DNA fragments expressing AtSGT1a, AtSGT1b, TPR-CSb (1–268), CS-SGSb (122–359), or CSb (122–268) were cloned into the *Eco*RI and *Not*I sites of pGEX-6P-1 (GST; Amersham Pharmacia Biotech) or pET28 (His_6, Novagen). Full-length *AtRAR1* and *CHORD-I* (1-77) were cloned into the *Eco*RI and *Xho*I sites of pGEX-6P-1 or pET28. The full-length cDNA products of *AtAHA1* (At3G12050) and *Atp23* (At3G03773) were cloned into pENTR and were recombined into pDEST15 (GST) and pDEST17 (His_6) using the GATEWAY SYSTEM. Full-length *TaHSP90* was cloned into pENTR. After site-directed mutagenesis, the *TaHSP90* clones in pENTR were recombined into pDEST17 (His_6) and pGWB (N-ter HA tag) using the GATEWAY SYSTEM. Site-directed mutagenesis was also performed using CSa-pGex-6p-1, AtSGT1a-pGEX-6P-1, and Myc-AtSGT1a-pBin61 in order to generate the E223K mutation.

Protein expression in *E. coli*.

The expression and purification of GST-AtRAR1 and His_6-AtRAR1 have been described previously (Heise *et al.* 2007). All the other GST and His_6 fusion proteins were expressed and purified from *E. coli* BL21 cells according to the manufacturer's protocol (Amersham Pharmacia Biotech and Novagen, respectively).

Plant materials and bacteria and virus strains.

The VIGS experiments and the transient expression system using transgenic *N. benthamiana* plants expressing Rx-HA under the control of its own promoter have been described elsewhere (Azevedo *et al*, 2006).

Dissociation constants estimation

Dissociation constants were estimated by fitting the titration curves with the Kaleidagraph software, using the following equation:

$$y = \Delta\delta_{\max} / 2c \times \left(K_d + x + c - \sqrt{(K_d + x + c)^2 - 4cx}\right)$$

where y is the weighted chemical shift displacement $\sqrt{\Delta\delta(^1H)^2 + 0.17 \cdot \Delta\delta(^{15}N)^2}$, x is the ligand concentration, c is the initial concentration of the protein (160 μM), $\Delta\delta_{max}$ is the maximum variation of the weighted chemical shift displacements and K_d is the estimated dissociation constant.

Modeling and Docking Simulation

The MODELLER program (Sali *et al*, 1993) was used to construct the structural models for the CS domain of AtSGT1a (code Q8W515) with the N-terminal domain of HSP90 (code P55737).

The template structures were for the CS domain of human SGT1 (PDB code 1RL1) and for the N-terminal domain of HSP90 (PDB code 2BYI), sharing a 38% and 77% sequence identity, respectively, with the target sequence. For each domain, a 1-ns molecular dynamic simulation at 300 K was carried out using the GROMACS v3.2 package (Van Der Spoel *et al*, 2005) (explicit solvent; OPLS force-field; and NVT ensemble). We selected 10 structures every 0.1 ns and used them as the starting structures for the docking procedure. The surface accessibility data calculated using the NACCESS program was used to define the so-called active and passive residues and the set of ambiguous distance restraints between them. From the experimental data, the active residues were selected as R153, E155, Y157, Q158, K159, F168, K170, K221, and E223 for the CS domain of AtSGT1A and E5, T86, K87, A88, D89, N92, N93, D144, and E145 for AtHSP90 (the sequence index of equivalent residues in ScHSP82 has been shifted by –1 and +1 in TaHSP90). Docking was performed using HADDOCK v1.3 (Dominguez *et al*, 2005). The target distance of these restraints was set as 2.0 Å; the force constants for empirical and experimental restraints were used as suggested by the default settings. Initially, 1000 structures for a CS/N-HSP90 complex were generated by docking one of the 10 models as rigid bodies, using only the ambiguous distance restraints, van der Waals' energy. Of these, 200 structures with the lowest overall energy were subsequently refined, allowing the side-chain conformations of the residues within the binding interface to be flexible. In a last iteration, refinement was performed by adding a layer of explicit solvent molecules and including the electrostatic component in the energy function.

Azevedo C, Betsuyaku S, Peart J, Takahashi A, Nöel L, Sadanandom A, Casais C, Parker J, Shirasu K (2006) Role of SGT1 in resistance protein accumulation in plant immunity. *EMBO J* **25:** 2007–2016

Dominguez C, Boelens R, Bonvin AM (2003) HADDOCK: a protein-protein docking approach based on biochemical or biophysical information. *J Am Chem Soc* **125:** 1731–1737

Heise CT, Le Duff CS, Böter M, Casais C, Airey JE, Leech AP, Amigues, B, Guerois R, Moore GR, Shirasu K, *et al* (2007) Biochemical characterization of RAR1 cysteine- and histidine-rich domains (CHORDs): a novel class of zinc-dependent protein-protein interaction modules. *Biochemistry* **46:** 1612–1623

Sali A, Blundell TL (1993) Comparative protein modelling by satisfaction of spatial restraints. *J Mol Biol* **234:** 779–815

Van Der Spoel D, Lindahl E, Hess B, Groenhof G, Mark AE, Berendsen HJ (2005) GROMACS: fast, flexible, and free. *J Comput Chem* **26:** 1701–1718

Supplementary Fig S1

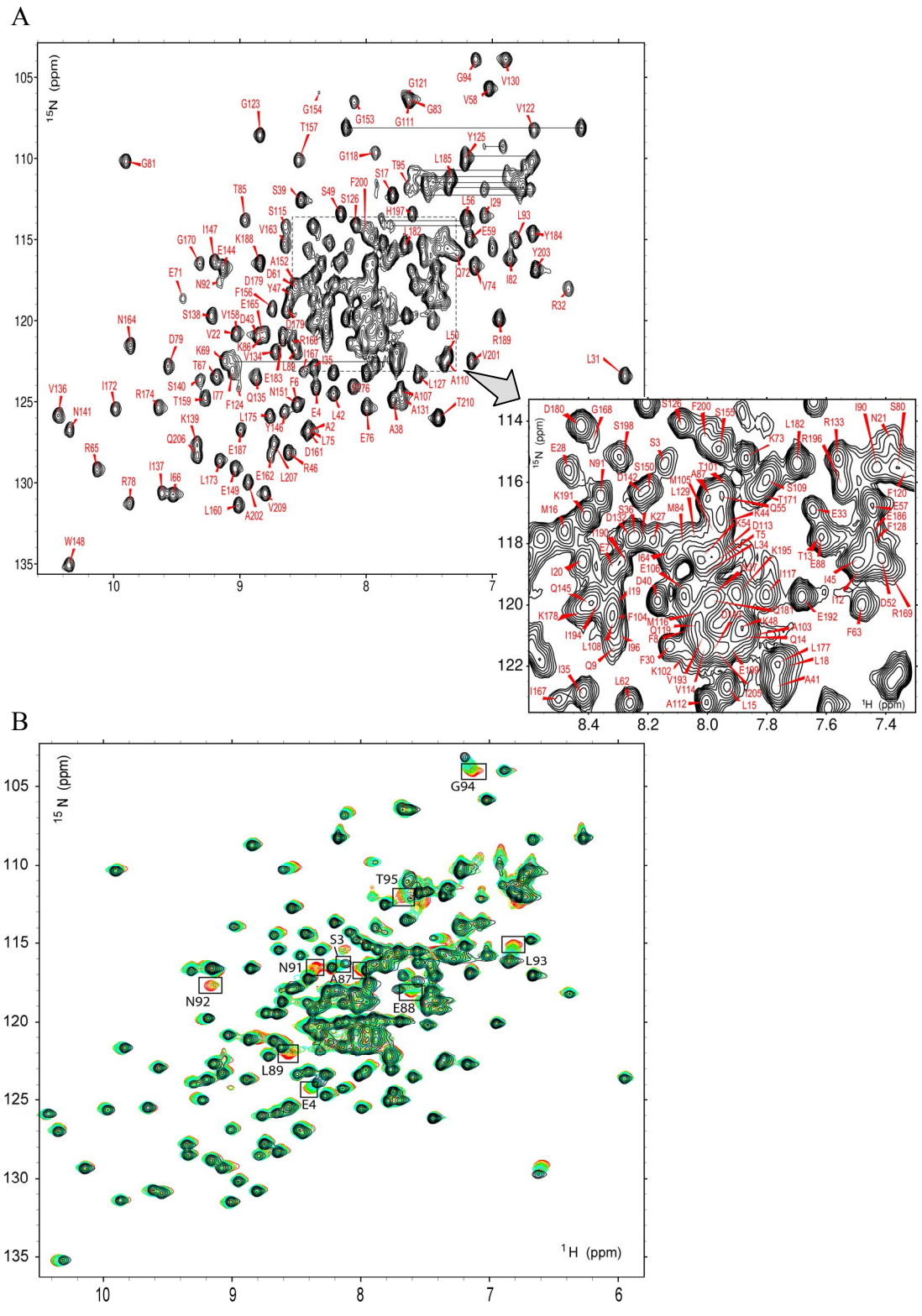

Fig S1| HSQC spectra of the N-terminal domain of *S. cerevisiae* HSP82 (N-ScHSP82) in the free and bound forms.

(A) The fully assigned HSQC spectrum of the free N-ScHSP82.

(B) Overlay of the N-ScHSP82 HSQC spectra obtained after adding increasing amounts of the CS domain of *S. cerevisiae* SGT1 up to a molar ratio of 1:0.5. The color code of the HSQC spectra is as follows: red (1:0), yellow (1:0.07), green (1:0.15), cyan (1:0.3), and black (1:0.5).

Supplementary Fig S2

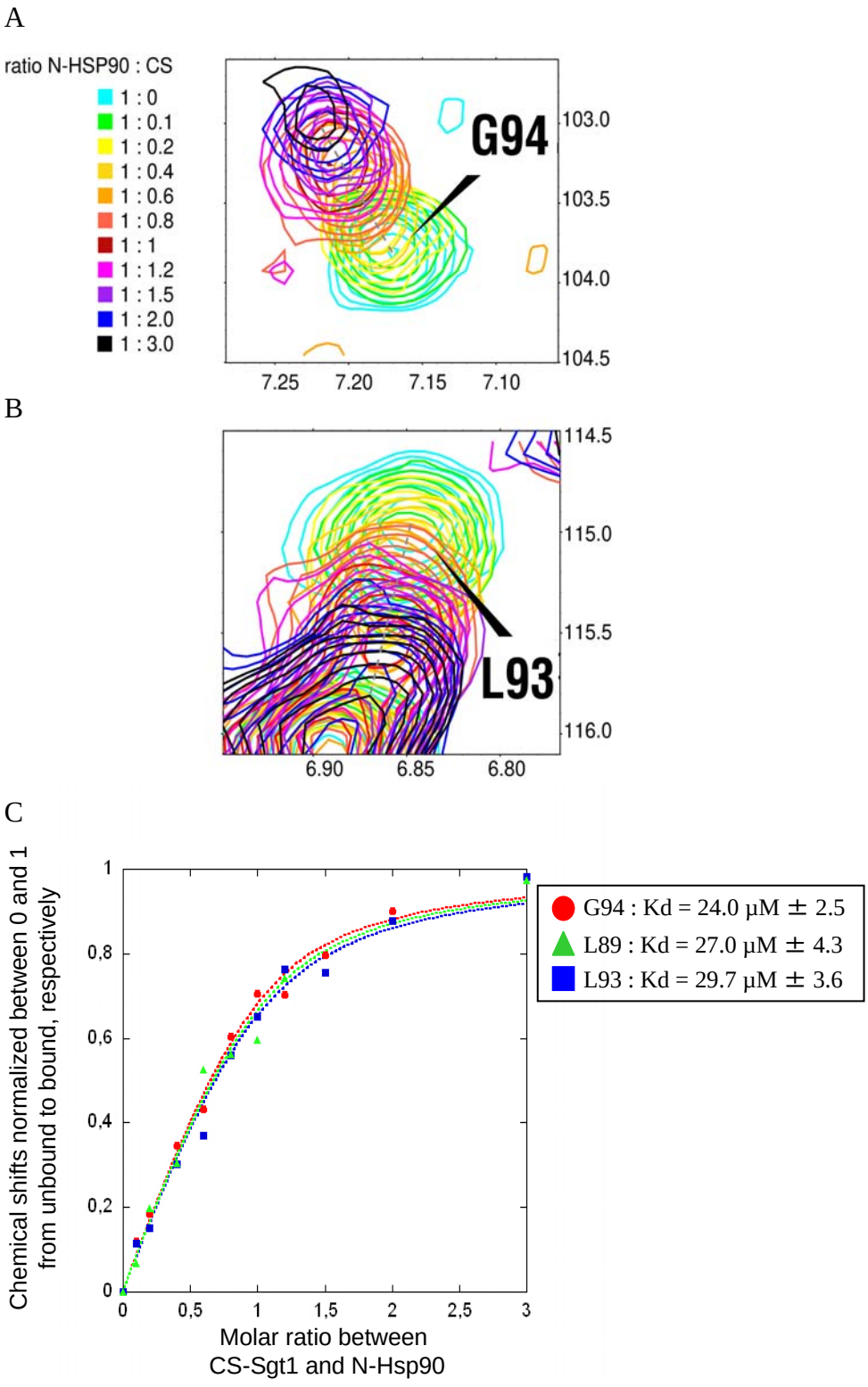

Fig S2| Estimation of the dissociation constant (Kd) between *S. cerevisiae* N-HSP82 and CS-SGT1 domains from the NMR titration using 15N labeled N-HSP82 domain. Zoom on (A) G94 and (B) L93 resonances along the titration from 1:0 to 1:3 molar ratios. The color code corresponding to the different molar ratio is provided on the side. (C) Plot of the variations of the chemical shifts of L89, L93 and G94 normalized with respect to the extreme values at 1:0 and 1:3 ratios. The fitted Kd are provided for the three residues from which a mean value of 27 µM can be derived.

Supplementary Fig S3

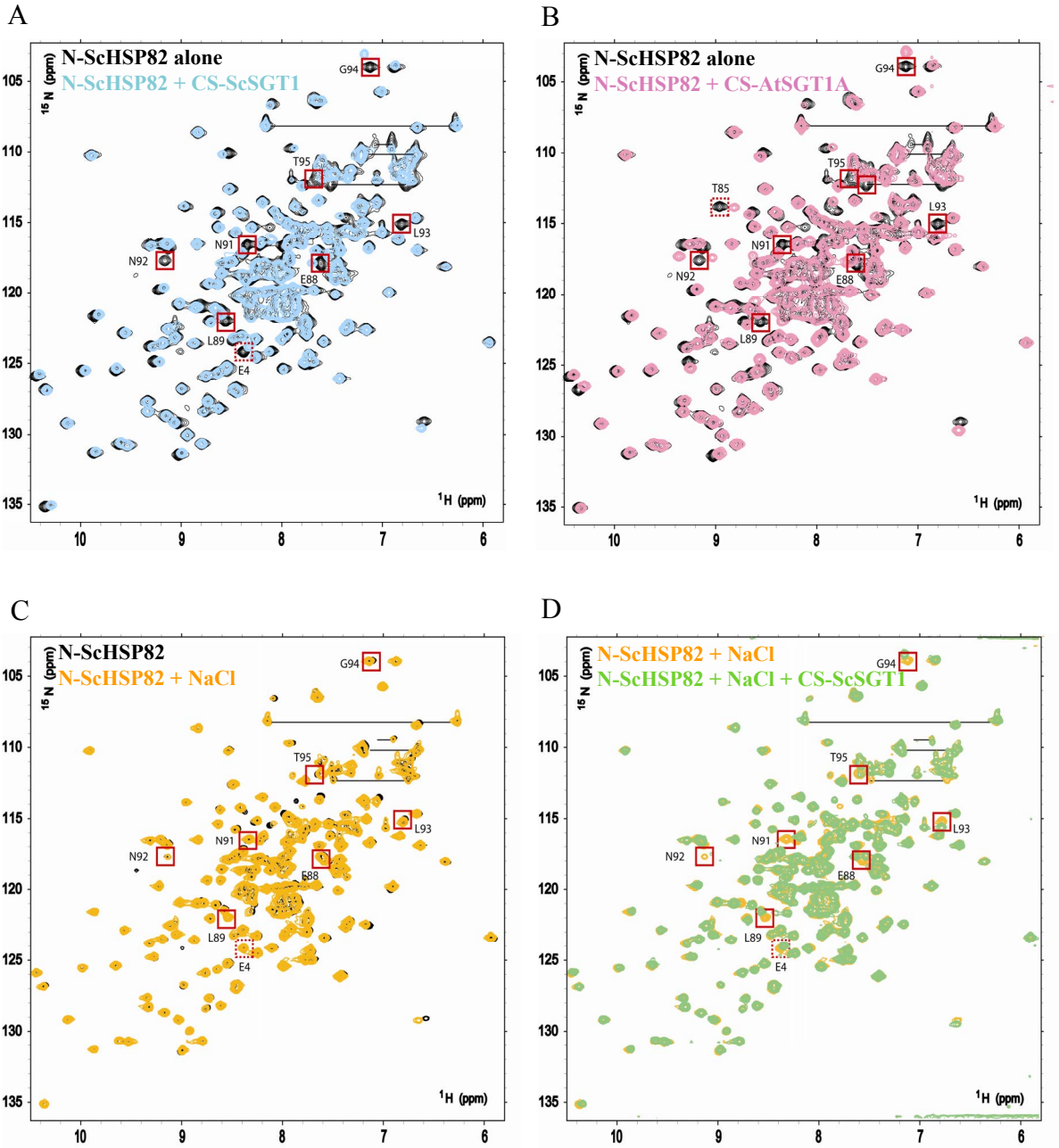

Fig S3| HSQC spectra of the N-terminal domain of *S. cerevisiae* HSP82 (N-ScHSP82) in presence of the *S. cerevisiae* CS-SGT1 or *Arabidopsis* CS-AtSGT1a domain. Superimposition of the HSQC spectra of the free N-ScHSP82 (black) and of the bound N-ScHSP82 in the presence of the *S. cerevisiae* (A) or *Arabidopsis* CS-AtSGT1a domain (B) at a molar ratio of 1:0.5. The squared correlations indicate those that disappear upon titration. (C) Superimposition of the HSQC spectra of the free N-ScHSP82 in the absence of salt (black) and with 150 mM NaCl (orange) showing no variation in the resonance. (D) The same resonances as in A were found affected upon addition of the CS domain at a 1:1 molar ratio (green) with respect to the free N-ScHSP82 in the presence of 150 mM NaCl.

Supplementary Fig S4

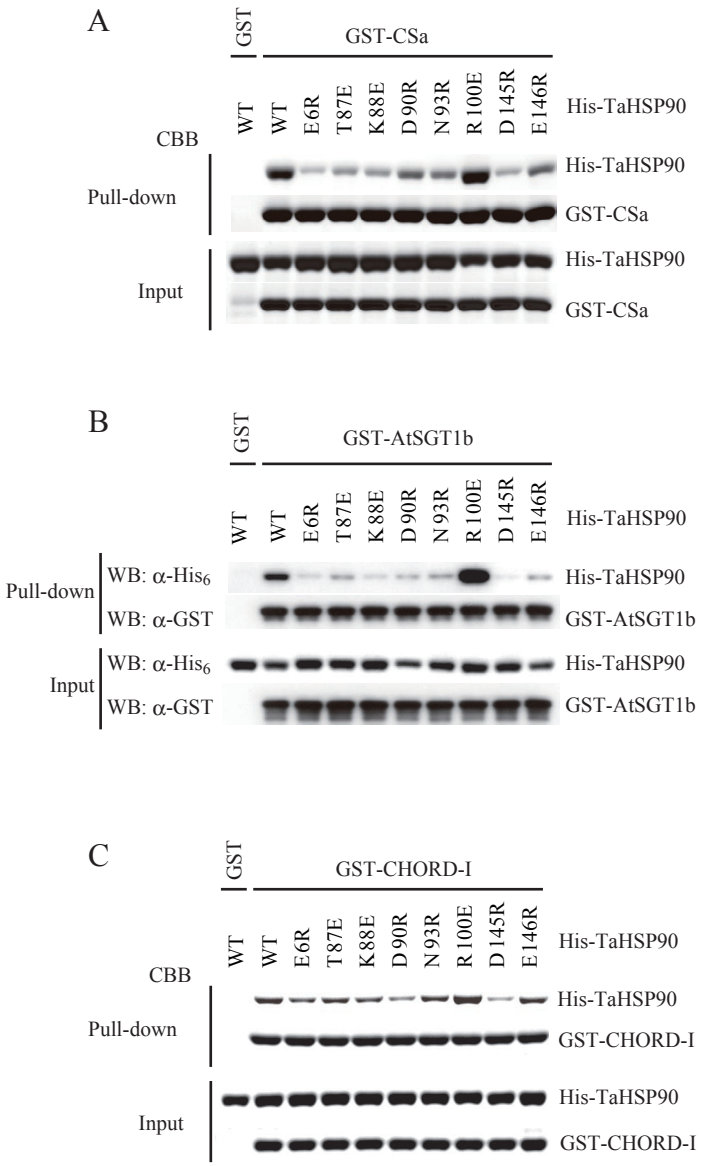

Fig S4| *In vitro* interaction assays of the CS domain of AtSGT1a (CSa), AtSGT1b, and CHORD-I with TaHSP90 mutants. GST-tagged CSa, GST-tagged AtSGT1b, or GST-tagged CHORD-I were incubated with purified His_6-TaHSP90 or mutants, and the pulled-down fractions were analyzed by SDS-PAGE followed by the Coomassie blue staining or immunoblotting using α-His_6 and α-GST antibodies as indicated. For the pull-down assay with GST-Atp23, 2 mM AMP-PNP was added to both the pull-down and washing buffers for enhancement of HSP90 binding.

Supplementary Fig S5

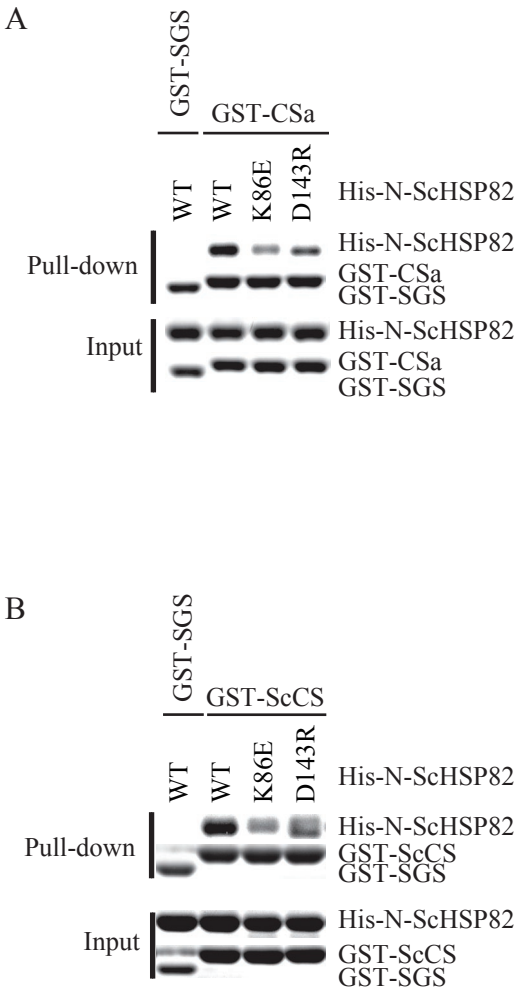

Fig S5| *In vitro* interaction assays of CSa, *S. cerevisiae* CS (ScCS) with N-terminal domain of *S. cerevisiae* HSP82 (N-ScHSP82) or mutants. GST-tagged CSa, or GST-tagged ScCS were incubated with purified His_6-N-ScHSP82 or mutants, and the pulled-down fractions were analyzed by SDS-PAGE followed by the Coomassie blue staining. GST-tagged SGS domain of AtSGT1b was used as a negative control.

Supplementary Fig S6

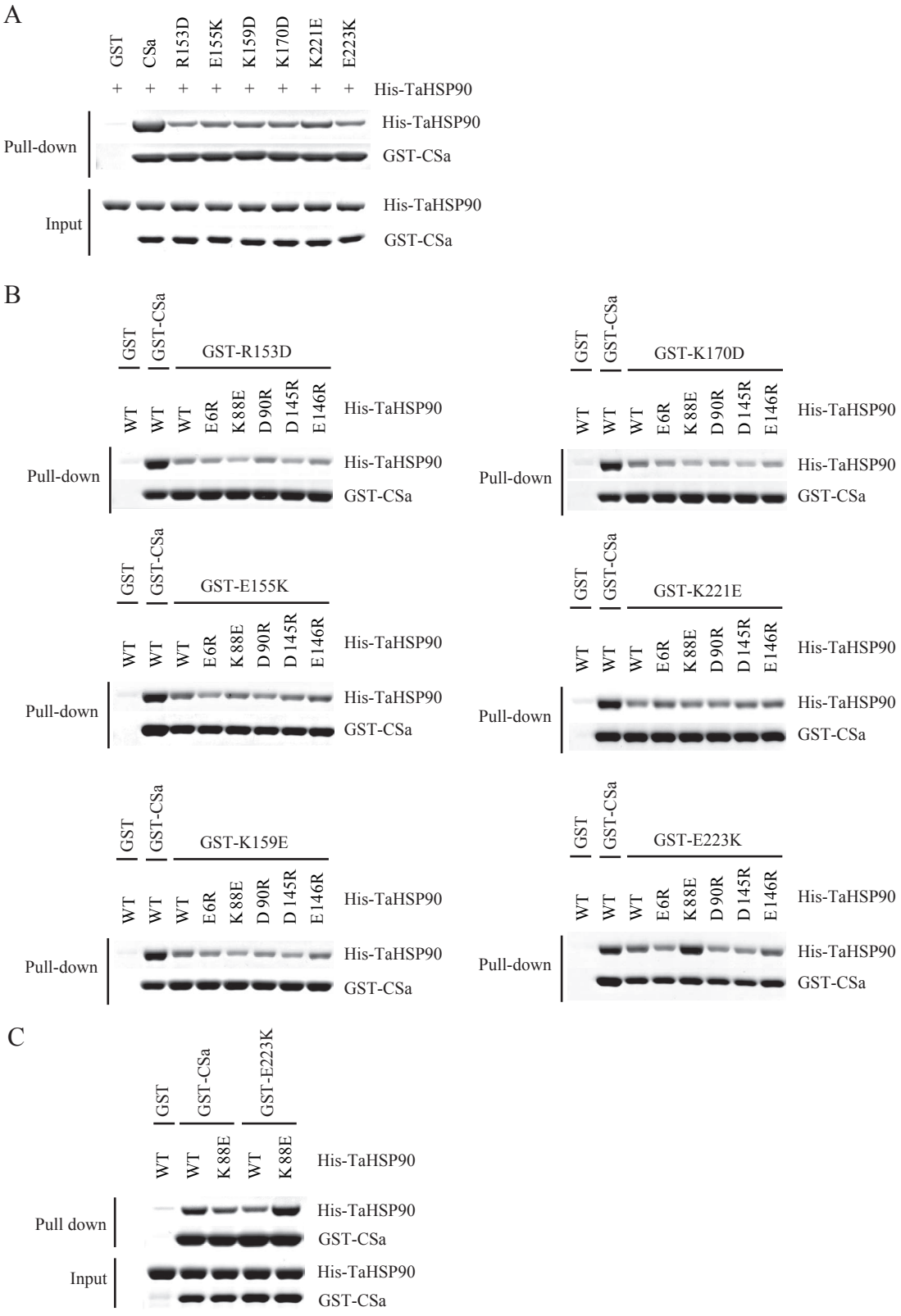

Fig S6| *In vitro* interaction assays between CSa and HSP90 mutants.
(A) *In vitro* interaction assays between CSa mutants and TaHSP90. GST-CSa or mutants were incubated with purified His_6-TaHSP90 as indicated, and the pulled-down fractions were analyzed by SDS-PAGE followed by the Coomassie blue staining. (B) GST-CSa or mutants (R153D, E155K, K159E, K170D, K221E, and E223K) were incubated with purified His_6-TaHSP90 or mutants (E6R, K88E, D90R, D145R, and E146R), and the pulled-down fractions were analyzed as shown in (A). (C) *In vitro* interaction assays between the K88E mutant of TaHSP90 and the E223K mutant of CSa. GST-CSa or GST-E223K in CSa was incubated with purified His_6-TaHSP90 or the His_6-K88E mutant of TaHSP90 as indicated, and the pulled-down fractions were analyzed as shown in (A).

Supplementary Fig S7

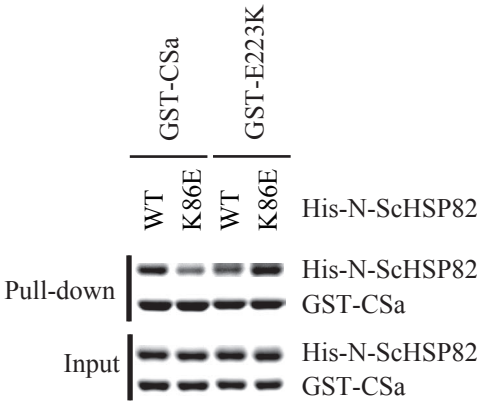

Fig S7| K86E mutation in N-terminal domain *S. cerevisiae* HSP82 (N-ScHSP82) complements the reduced binding of E223K mutation in CSa. GST-CSa or GST-E223K in CSa was incubated with purified His_6-N-ScHSP82 or the His_6-K86E mutant of N-ScHSP82 as indicated, and the pulled-down fractions were analyzed by SDS-PAGE followed by the Coomassie blue staining.

Supplementary Fig S8

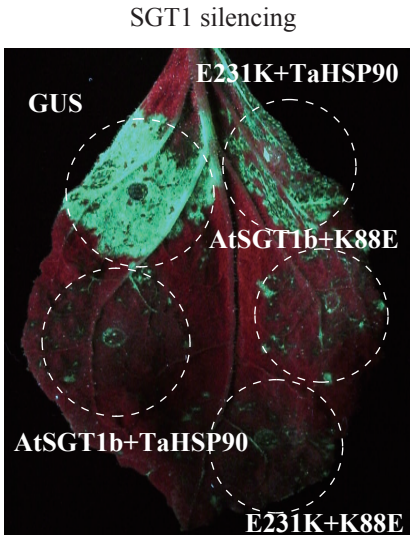

Fig S8| The K88E mutation in HSP90 complements the loss of function of the E231K mutant of AtSGT1b for defence response against PVX. *Myc-AtSGT1b* or *Myc-E231K* and *HA-TaHSP90* or *HA-K88E* were coexpressed with *PVX-GFP* by *Agrobacterium* (OD 0.3, 0.3, and 0.001) in Rx-containing *N. benthamiana* plants silenced for *NbSGT1*. After 4–7 d, PVX-GFP accumulation was monitored by GFP fluorescence under UV light.

Supplementary Fig S9

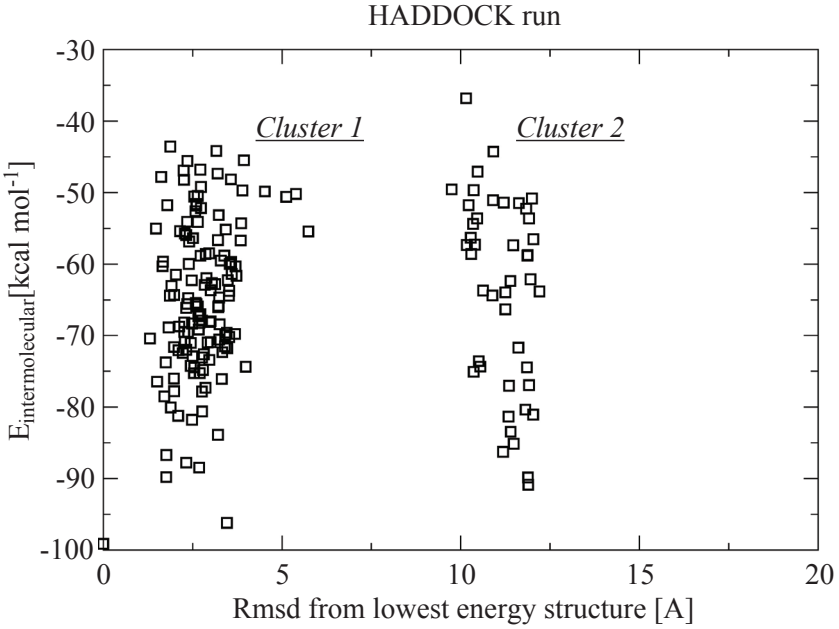

Fig S9| Docking and clustering analysis. Intermolecular energies of the 200 complex models docked using the HADDOCK software plotted against their RMSD with the lowest energy complex. Intermolecular energies are calculated as the sum of the van der Waals term and the electrostatic energies weighted with weighting factors 1 and 0.1, respectively. The model selected to create the Figure 4 in the manuscript correspond to the lowest energy structure of the cluster 1.

Supplementary Fig S10

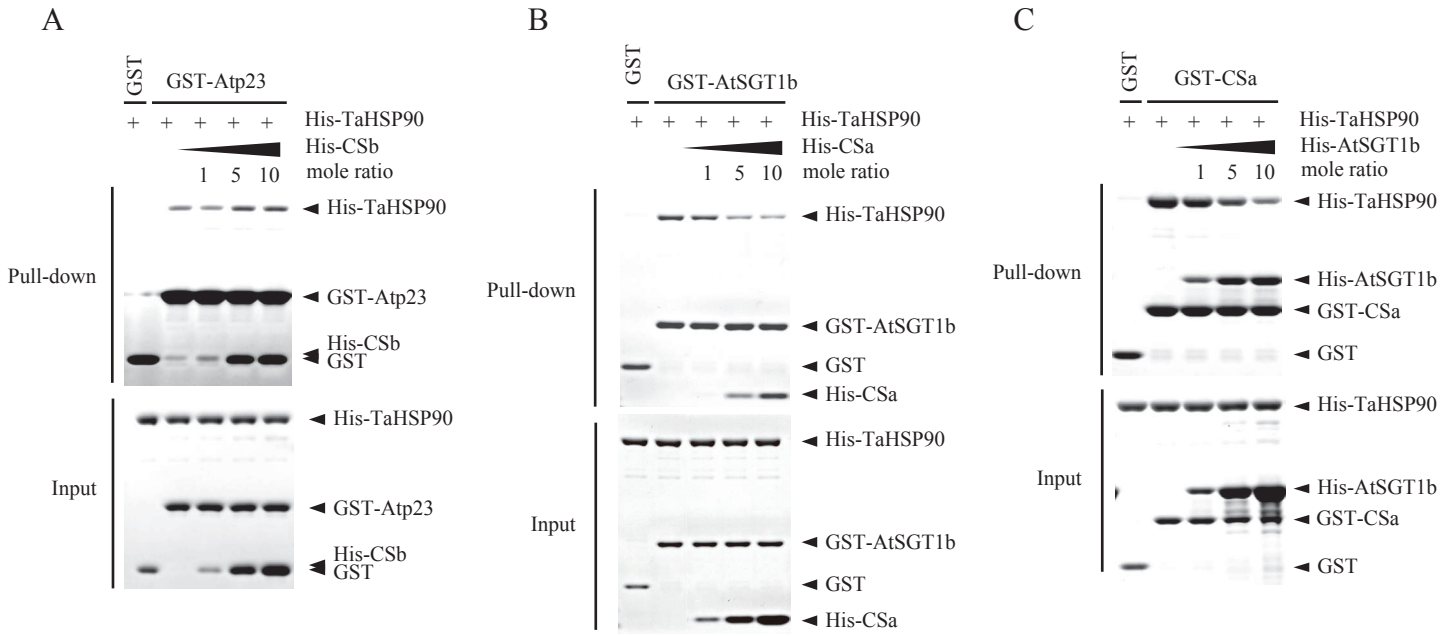

Fig S10| Competition assay between CSb and Atp23 for binding to HSP90.
(A) CSb did not compete with Atp23 for binding to TaHSP90. (B) Full-length AtSGT1b competed with CSa for binding to TaHSP90. (C) CSa competed with AtSGT1b for binding to TaHSP90. GST-Atp23, GST-SGT1b, or GST-CSa were incubated with His_6-TaHSP90 in the absence or presence of increasing amounts of purified His_6-CSa or His_6-AtSGT1b as indicated. For the pull-down assay with GST-Atp23, 2 mM AMP-PNP was added to both the pull-down and washing buffers. The GST-pulled down fractions were analyzed by SDS-PAGE and the Coomassie blue staining.

Supplementary Fig S11

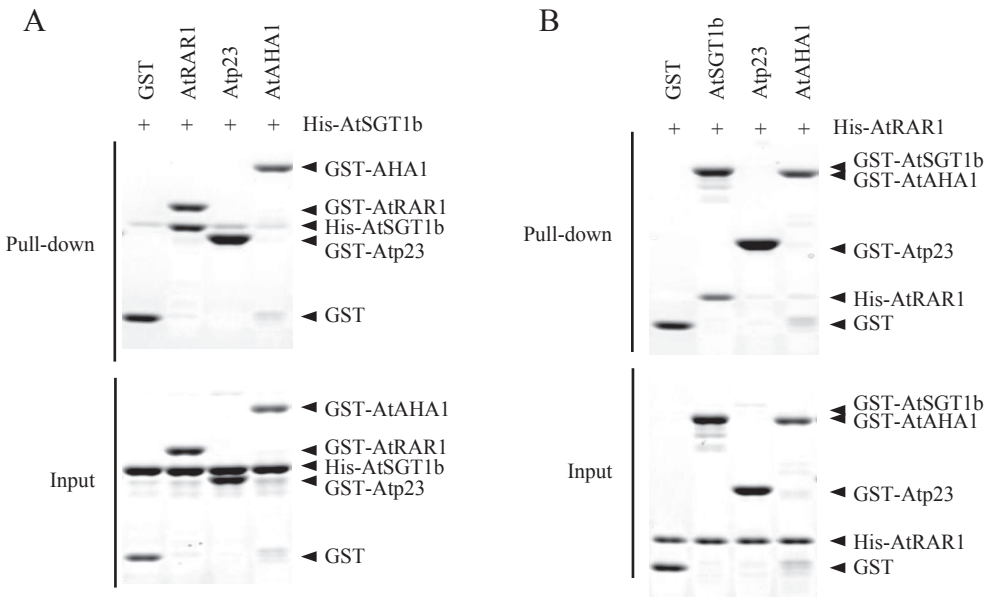

Fig S11| *In vitro* interaction assays between SGT1b or RAR1 and Atp23 or AtAHA1. (A) Atp23 and AtAHA1 did not interact with AtSGT1b. GST-AtRAR1, GST-Atp23, and GST-AtAHA1 were incubated with His_6-AtSGT1b. (B) Atp23 and AtAHA1 did not interact with AtRAR1. GST-AtSGT1b, GST-Atp23, and GST-AtAHA1 were incubated with His_6-AtRAR1. The GST-pulled down fractions were analyzed by SDS-PAGE and the Coomassie blue staining.

Supplementary Fig S12

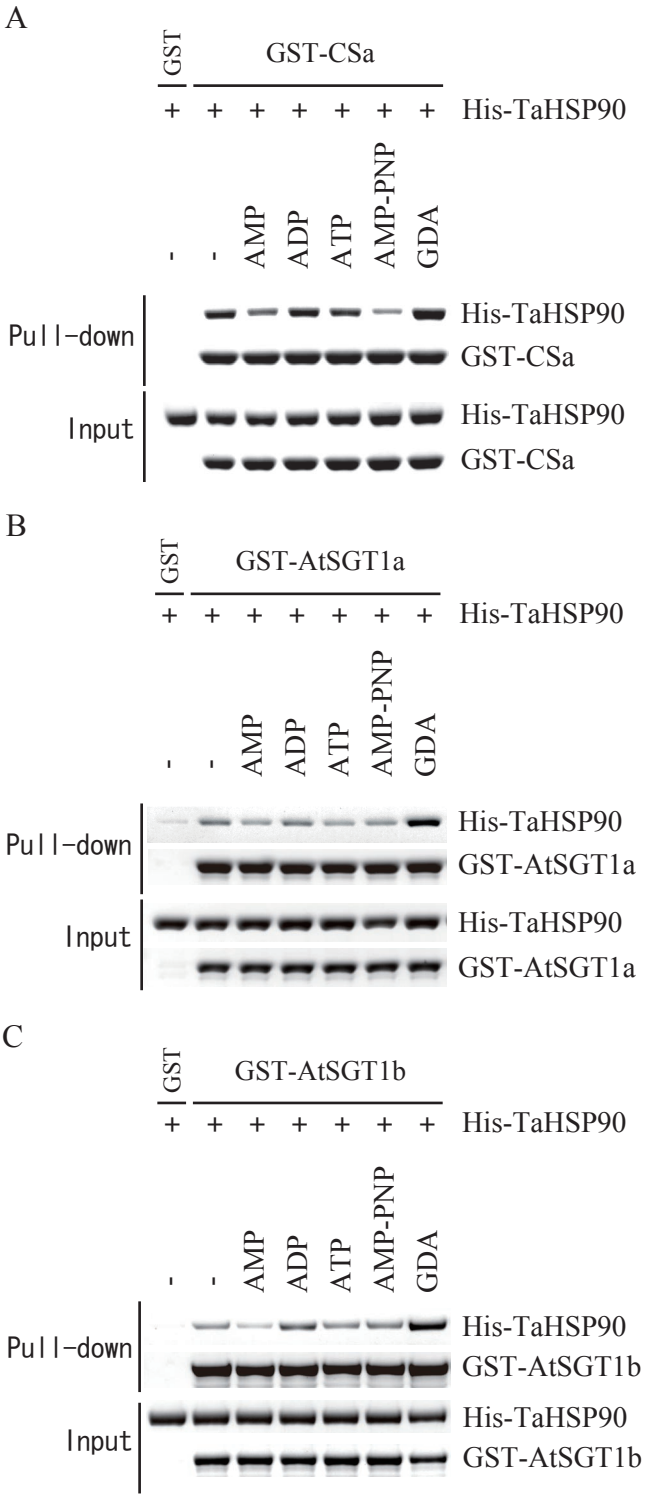

Fig S12| Nucleotide dependence of CSa, AtSGT1a, and AtSGT1b for binding to HSP90. GST-CSa, GST-AtSGT1a, and GST-AtSGT1b were incubated with purified His_6-TaHSP90 and with 5 mM of various nucleotides or 20 μM geldanamycin (GDA) as indicated, and the pulled-down fractions were analyzed by SDS-PAGE followed by the Coomassie blue staining.